

Published in final edited form as:

Nat Struct Mol Biol. 2012 December ; 19(12): 1293–1299. doi:10.1038/nsmb.2416.

Neuropilins lock secreted semaphorins onto plexins in a ternary signaling complex

Bert J.C. Janssen^{1,3,*}, Tomas Malinauskas^{1,*}, Greg A. Weir², M. Zameel Cader², Christian Siebold¹, and E. Yvonne Jones^{1,#}

¹Division of Structural Biology, Wellcome Trust Centre for Human Genetics, University of Oxford, Oxford, United Kingdom

²Medical Research Council Functional Genomics Unit, Department of Physiology, Anatomy and Genetics, University of Oxford, Oxford, United Kingdom

Abstract

Co-receptors add complexity to cell-cell signaling systems. The secreted semaphorin 3s (Sema3s) require a co-receptor, neuropilin (Nrp), to signal through plexin As (PlxnAs) in functions ranging from axon guidance to bone homeostasis, but the co-receptor's role is obscure. Here we present the low resolution crystal structure of a mouse semaphorin-plexin-Nrp complex alongside unliganded component structures. Dimeric semaphorin, two copies of plexin and two copies of Nrp are arranged as a dimer of heterotrimers. In each heterotrimer sub-complex semaphorin contacts plexin as in co-receptor independent signaling complexes. The Nrp1s cross-brace the assembly, bridging between sema domains of the Sema3A and PlxnA2 subunits from the two heterotrimers. Biophysical and cellular analyses confirm that this Nrp binding mode stabilizes a canonical, but weakened Sema3-PlxnA interaction, adding co-receptor control over the mechanism by which receptor dimerization and/or oligomerization triggers signaling.

Keywords

cell-cell signaling; axon guidance; ternary complex; crystal structure

The interplay of multiple intercellular signaling systems is essential for organogenesis and tissue homeostasis. These systems include extracellular cues to provide attractive and repulsive cell guidance effects. Members of several protein families serve as guidance cues, binding to cell surface receptors to trigger discrete changes in the cytoskeleton. Many of these guidance cues were initially characterized in studies of the mechanisms that direct neuronal wiring during the development of the nervous system¹. However, protein families

[#]to whom Correspondence and request for materials should be addressed to E.Y.J. (yvonne@strubi.ox.ac.uk).

³Present address: Crystal and Structural Chemistry, Bijvoet Center for Biomolecular Research, Department of Chemistry, Faculty of Science, Utrecht University, Utrecht, The Netherlands

*These authors contributed equally to this work

Author Contributions

B.J.C.J., T.M., C.S. and E.Y.J. designed the project. B.J.C.J. and E.Y.J. wrote the manuscript with input from all authors. B.J.C.J. produced the constructs for crystallization, performed MALS, crystallization, diffraction data collection, structure solution and refinement. T.M. and B.J.C.J. cloned and produced constructs for SPR experiments and performed SPR experiments. T.M. did the Western blot analysis. T.M. produced proteins for growth cone collapse assays which G.A.W. performed under supervision of M.Z.C.

Note: Supplementary information is available in the online version of the paper.

Competing interests. The authors declare no competing financial interests

Coordinates and structure factors for Nrp1₁₋₄, Sema3A_{S-F}-PlxnA2₁₋₄-Nrp1₁₋₄ and Sema3A_{S-p-I} have been deposited in the Protein Data Bank with accession numbers 4GZ9, 4GZA and 4GZ8, respectively.

first identified as guidance cues steering neuronal growth cones are now implicated in a plethora of physiological functions which require changes in cellular morphology². The semaphorins comprise one of the largest of these families of guidance cues and occur in secreted or cell attached forms in multicellular organisms ranging from *Caenorhabditis elegans* to humans²⁻³. Semaphorins are important for the development and function of myriad tissues. For example, numerous roles have to date been reported for semaphorins in the immune system, cardiac development and cancer biology, in addition to a range of activities in neural systems which extend well beyond the actions on axonal growth cones by which family members were first identified as repulsive guidance cues²⁻⁵. The majority of semaphorin functions utilize members of the plexin family of cell surface receptors for signal transduction, however, for many systems plexins cannot alone function as semaphorin receptors, but rather act as part of a holoreceptor, a receptor complex which includes one (or more) co-receptors²⁻³.

The widely studied class 3 semaphorins (Sema3A to G) are the only secreted semaphorins in vertebrates (Fig. 1a). Numerous Sema3 functions depend on signaling through one of the A class plexins (PlxnA1 to 4), receptors also used by the membrane associated Sema6s². The interactions between Sema6s and PlxnAs are direct, formed through conserved contacts of the N-terminal seven-bladed β -propeller (sema) domains of both semaphorin and plexin⁶⁻⁷. In contrast, Sema3 signaling depends on the semaphorin interacting with one of two Nrp (Nrp1 or 2) co-receptors which associate with the PlxnA to generate holoreceptors⁸⁻¹¹. The Nrps are single transmembrane-spanning cell surface glycoproteins which, in addition to their role in Sema3 holoreceptors, serve as isoform-specific co-receptors for vascular endothelial growth factor (VEGF) and as such are involved in vascular development and tumorigenesis¹².

An N-terminal seven-bladed β -propeller sema domain followed by a cysteine-rich PSI (plexin, semaphorin, integrin) domain is a signature feature in the ectodomains of semaphorin and plexin family members^{6-7,13-15}. The composition of the remainder of the semaphorin ectodomain varies according to class; the ectodomains of the secreted class 3 semaphorins contain an immunoglobulin-like (Ig) domain and basic C-terminal tail (Fig. 1a). The crystal structure of the sema domain of Sema3A has been determined¹³ and shows a homodimer, in common with the crystal structures of unliganded SEMA4D, Sema6A and A39R, a viral mimic of SEMA7A^{6-7,14-15}. The ectodomains of plexins contain additional PSI domains plus IPT (Ig domain shared by plexins and transcription factors) domains (Fig. 1a). The crystal structure of the N-terminal four domains of PlxnA2 (sema-PSI1-IPT1-PSI2) has been determined and, in contrast to the semaphorins, the sema domain of the unliganded plexin shows little or no propensity to homodimerize⁶⁻⁷. Recent crystal structures have revealed the generic architecture of co-receptor independent semaphorin-plexin interactions^{6-7,15} and alongside studies of plexin intracellular regions (most recently¹⁶⁻¹⁹) indicate that semaphorin induced dimerization and possibly oligomerization of the plexin cytoplasmic region triggers signaling.

The Nrps, Nrp1 and Nrp2, have ectodomains comprising two N-terminal CUB domains (also termed a1 and a2), two coagulation factor V/VIII homology domains (termed domains b1 and b2) and a membrane proximal MAM domain (termed domain c) (Fig. 1a). The c domain has been reported to mediate Nrp dimerization but not to interact directly with either semaphorin or VEGF ligands²⁰⁻²². The most extensive structure determined for the Nrp ectodomain is of NRP2 a1-a2-b1-b2 in complex with a Fab fragment of an antibody known to inhibit Sema3 binding²³. This crystal structure revealed the Fab fragment binding involves only the a1 domain of NRP2 a1-a2-b1-b2. No structures have been reported to date for Nrps in complex with semaphorin ligands.

Sema3A-Nrp1 signaling through PlxnA has antitumorigenic activity and controls many aspects of neuronal development²⁴, for example, Sema3A-Nrp1-PlxnA2 signaling repulses sensory axons²⁵ and guides migration of neurons in the cortex²⁶. To address the role and effect of Nrps on how Sema3 and PlxnA class members signal, we characterized the Sema3A_{S-P}-PlxnA2₁₋₄-Nrp1₁₋₄ complex as well as the individual proteins both structurally and functionally (see Fig. 1a for domain organization and definition of nomenclature).

RESULTS

Nrp1₁₋₄ crystal structure

Functional analyses have identified the N-terminal four domains of Nrp as the extracellular region which mediates co-receptor interactions^{13,20-23}. We have determined the crystal structure of Nrp1₁₋₄ to 2.7 Å resolution (see Table 1). In the structure, the a1 domain protrudes away from the a2-b1-b2 domain structural unit with which it interacts only via a three residue linker (Fig. 1b). This separation distinguishes a1 in terms of increased surface accessibility and potential for positional mobility relative to a2-b1-b2. Indeed, superposition with the previously reported crystal structure of human NRP2 a1-a2-b1-b2 (ref. 23) revealed a high level of structural similarity except for the relative positions of the a1 and a2-b1-b2 units; presumably the Nrp1 and NRP2 crystal lattices have sampled two different alternatives from what is a wide range of possible a1 orientations common to both Nrps (Supplementary Fig. 1a). In our Nrp1₁₋₄ structure each of the two canonical CUB domain (a1 and a2) calcium binding sites is occupied by a calcium ion. Similar to NRP2₁₋₄ (ref. 23) Nrp1₁₋₄ is monomeric in solution¹³ (Supplementary Fig. 1b) and the packing in the crystal lattice provides no indications of oligomer formation.

Nrp1₁₋₄, PlxnA2₁₋₄ and Sema3A_{S-P} form a ternary complex

Nrp1₁₋₄, PlxnA2₁₋₄ and Sema3A_{S-P} interacted with highest apparent affinity when we tested them together in surface plasmon resonance (SPR) assays (Fig. 1c and Supplementary Fig. 2). Sema3A_{S-P} alone did not give any measurable indication of binding PlxnA2₁₋₄ to concentrations of at least 73 μM. This interaction has also been reported to be undetectable in cell binding assays using dimerized Sema3A, tested to concentrations of at least 10 nM¹¹. Conversely, in our SPR assays, Sema3A_{S-P} and Nrp1₁₋₄ interacted directly, in agreement with previous biophysical and cell based analyses⁸⁻⁹. Nrp1₁₋₄ also bound directly to PlxnA2₁₋₄ with a dissociation constant (K_d) of 66 μM (Fig. 1c), indicating that, even in the absence of semaphorins, Nrps and PlxnAs may coexist as complexes on the cell-surface, consistent with observations from numerous functional studies (for example²⁷). The higher apparent affinity on concurrent interaction of all three components probably arises from a simple additive effect of the individual interactions and suggests that a ternary complex is formed containing all three components (although we cannot formally exclude scenarios involving induced conformational changes).

Ternary complex crystal structure

We have determined the crystal structure of the ternary complex consisting of Sema3A_{S-F} (see Methods and Fig. 1 for construct details), PlxnA2₁₋₄ and Nrp1₁₋₄ to 7.0 Å resolution. Our structure determination of this low resolution complex was aided by the availability of high resolution structures of the individual components (2.3 Å PlxnA2₁₋₄, 2.8 Å Sema3A_S and 2.7 Å Nrp1₁₋₄; refs^{6,13} and this study, respectively). We searched for individual molecules incrementally by molecular replacement (see Methods and Supplementary Fig. 3), this procedure yielded a final solution for the crystal content comprising the ternary complex, positioned on a two-fold axis, plus five unliganded PlxnA2₁₋₄ molecules. The presence of clear electron density for molecules excluded from the molecular replacement solution (Supplementary Fig. 3) and the low R_{work}/R_{free} values (28.5/28.5%, see Table 1)

after rigid body refinement provide robust support for this structure solution. The sema domains of semaphorin and plexin molecules share a seven-bladed β -propeller topology, but have substantial, distinctive, differences in structure^{6-7,15}. For the avoidance of doubt, we tested, using the program PHASER²⁸, whether the semaphorin and plexin sema domains could be positioned interchangeably in our crystal structure. We found that the structural differences were indeed sufficient to render the positions of semaphorin and plexin sema domains clearly distinguishable as were the β -strand based structures of the plexin IPT and Nrp a1 domains. We examined the environment of each of the unliganded PlxnA2₁₋₄ molecules within the crystal lattice and found that packing contacts precluded bivalent binding of Sema3A_{S-F} at these positions. We could only place Nrp1 domain a1 unequivocally in the ternary complex. Despite the presence of the entire Nrp1₁₋₄ protein in the complex crystal and lack of proteolytic processing (Supplementary Fig. 4), the Nrp1 a2-b1-b2 structural unit could not be located, indicating substantial mobility between a1 and the a2-b1-b2 moieties.

Nrp1 cross-braces apposing semaphorin-plexin pairings

The Sema3A_{S-F}-PlxnA2₁₋₄-Nrp1₁₋₄ complex is organized around a crystallographic two-fold axis. At the core of the assembly each subunit of the Sema3A dimer binds a PlxnA2 molecule, such that semaphorin and plexin interface via their respective N-terminal sema domains (Fig. 2a). The a1 domains of two Nrp1 molecules serve as cross-braces for the overall complex, each wedged between the sema domain of the Sema3A subunit from one semaphorin-plexin pairing and the sema domain of the PlxnA2 molecule from the other pairing. Although the low resolution of the crystal structure precludes detailed analysis of local mainchain and sidechain conformations there are clearly no large conformational changes upon complex formation. The Sema3A dimer in the complex remains very similar to the previously reported structure of unliganded Sema3A¹³; only small differences in domain orientation are apparent (Supplementary Fig. 5a). Similarly, there are only minor changes of domain orientation within PlxnA2₁₋₄ (Supplementary Fig. 5b,c). The positioning of the Nrp1, locking the components of apposing semaphorin-plexin pairings within the overall structure, provides an explanation for the essential contribution of this co-receptor to formation of the signaling capable complex.

Semaphorin – plexin complexes are structurally similar

The arrangements and positions of Sema3A and PlxnA2 in the ternary complex are very similar to the recently reported structures of semaphorin-plexin complexes that do not require a co-receptor for signaling, namely Sema6A-PlxnA2⁶⁻⁷, SEMA4D-PLXNB1 (ref. 6) and SEMA7A-PLXNC1 (ref. 15) (Fig. 2b and Supplementary Fig. 5d). All the complexes use equivalent sites on plexin and semaphorin for interaction. The Sema3A-PlxnA2 interface architecture shows a striking similarity with that of Sema6A-PlxnA2 despite only 34% sequence identity between Sema3A and Sema6A (Fig. 2b). The binding site of Nrp1 on Sema3A is predominantly formed by the extrusion (a 70 residue insert within sema domain blade 5 (ref. 14) consisting of residues 345-419 in Sema3A). The Sema3A-PlxnA2, Nrp1-Sema3A and Nrp1-PlxnA2 interfaces show high levels of sequence conservation (Fig. 2c,d,e) and consist of mixed charged and hydrophilic interactions (i.e. Sema3A-Nrp1 predominantly neutral, PlxnA2-Nrp1 slightly charged, PlxnA2-Sema3A mixed charged-hydrophilic). The lack of Sema6A interaction with Nrp1²⁹ may be due to steric clashes arising from loops 357-360 and/or 371-377 in the extrusion which are larger and structurally different in Sema6A, or from single residue differences (such as Sema3A Y375 versus Sema6A K363) to those in the Nrp1 binding interface on Sema3A (Supplementary Fig. 5e). Similarly, in the Sema3A-PlxnA2 interface one or a combination of a few critical residue substitutions may cause the much reduced affinity of Sema3A compared to Sema6A for PlxnA2 (refs. 6-7).

Sema3 activity can be fine-tuned through several internal furin processing sites³⁰. Cleavage of Sema3A at an internal furin site in the PSI domain reduces activity. The Sema3A we used for the ternary complex crystal structure (Sema3A_{S-F}), and the previously reported Sema3A crystal structure¹³, terminate at or about this cleavage site. We therefore also determined the crystal structure of Sema3A_{S-P-I}, to 3.3 Å resolution (see Table 1), using a construct (Sema3A_{S-P-I}; Fig. 3a) in which the furin cleavage site is mutated to prevent processing (R551A and R555A; see Methods). In the electron density maps we calculated for Sema3A_{S-P-I} there was clear electron density for the sema and PSI domains but the IG domain appeared largely disordered, thus we were only able to build a partial structure for this domain and did not assign any residue sequence (Fig. 3a). The structure of Sema3A_{S-P-I} is very similar to that of unliganded Sema3A_S¹³ and to Sema3A_{S-F} from the Sema3A-PlxnA2-Nrp1 complex. In these two Sema3A variants the PSI domain is disordered probably because it is only partially present in the protein. Superposition of the cleaved and un-cleaved Sema3A structures reveals no large differences in the sema domain dimer (Fig. 3b), thus excluding conformation-based effects of furin cleavage on activity. Our Sema3A_{S-P-I} crystal structure also provides some additional information on the overall architecture of Sema3A. Superposition of Sema3A_{S-P-I} and SEMA4D_{S-P-I}¹⁴ reveals the similarity between these two structures (Fig. 3c; rmsd of 1.6 Å, over 1032 Cα atoms). Our crystal structures provide no direct information on the putative Nrp b1 domain binding site in the Sema3 C-terminal region³¹, however, modeling indicates that, given the mobility provided by the linker regions in the Nrp and the Sema3 C-terminal basic region, this additional interaction could be accommodated within the ternary structure (data not shown).

Overall the similarity in complex architecture of Sema3A-PlxnA2-Nrp1 with those of other semaphorin-plexin combinations that do not use Nrp as a co-receptor suggests that the mechanisms triggering signaling are in essence conserved.

Biophysical and cellular analyses support structural data

The architecture and interfaces of the ternary complex correlate well with previous functional observations, however, we sought to provide additional experimental confirmation of their biological relevance. We selected for individual mutation sequences which were surface exposed in the unliganded structures and which sampled each of the interfaces in our ternary complex (with the exception of the Sema3A-PlxnA2 interface). Given the low resolution of the structural information guiding our choice of residues, we designed mutations to introduce asparagine-linked glycosylation sites; an N-linked glycan would be predicted to provide substantial steric hindrance to interface formation. We used mutant proteins which were secreted at similar levels to the wild type molecules in our mammalian cell based expression system (see Methods) for binding assays. We found that introduction of an N-linked glycosylation site in PlxnA2₁₋₄ F275N (on the basis of the complex structure a site predicted to hinder Nrp binding; Fig. 2c), in Nrp1₁₋₄ P73A H74S (predicted to hinder Sema3A binding; Fig 2c) and in Sema3A_{S-P} L353N P355S (predicted to hinder Nrp1 binding; Fig 2c) resulted in weaker interactions between the component proteins in SPR-based binding assays (Fig. 4a and Supplementary Fig. 6). Sema3A_{S-P} L353N P355S also inhibited dorsal root ganglion (DRG) growth cone collapse (Fig. 4b,c). The architecture of the ternary complex positions the calcium binding site in the α1 domain of Nrp1 at the interface with PlxnA2 and in proximity to the binding site for Sema3A suggesting that it provides structural integrity and/or shields negative charges that would prevent interaction. This prediction concurs with our findings that calcium ions were required for ternary complex interactions in our SPR experiments (Fig. 4a and Supplementary Fig. 6d) and were needed for growth cone collapse induced by Sema3A²³.

Several previously reported Sema3A mutations that result in loss-of-function *in vitro* and *in vivo*, but that retain their ability to bind Nrp1 (refs. 7,32), map to the Sema3A-PlxnA2

interface and do not impinge on that of *Sema3A-Nrp1* (Fig. 2d). A peptide consisting of *Sema3A* extrusion loop residues 363-380 binds *Nrp1* (ref. 33) and an antibody generated against this peptide inhibits *Sema3A* function³⁴⁻³⁵; a large part of this *Sema3A* loop contributes to the *Nrp1* binding site in our complex structure (Fig. 2d). On the other hand, we were unable to demonstrate that *Nrp1* domain a1 on its own is sufficient for binding to *Sema3A* or to *Sema3A-PlxnA2* in our SPR assays (the *Nrp1* a2-b1-b2 domain combination also showed no measurable binding) (Supplementary Fig. 6). It seems that the *Nrp1* four domain combination is needed for sufficiently stable complex formation (Fig. 1c) and, although not observed in the crystal structure, we therefore currently cannot exclude a direct contribution of *Nrp1* domains a2-b1-b2. The importance of *Nrp1* domain a1 in complex formation and signaling has, however, been shown by others. The interaction site of an antibody against *Nrp1* domain a1 that inhibits *Sema3A* function and prevents *Sema3A-Nrp1* interaction²³ correlates well with the *Sema3A* binding site on *Nrp1* that we observed in the ternary complex (Fig. 2c,d). In addition, *Nrp1* site-directed mutants that disrupt *Sema3A* interactions are in or near the *Sema3A* interface in our complex structure, whereas mutations that do not affect *Sema3A* binding³⁶ are indeed outside those interfaces (Fig. 2c). Thus, our structural data are supported by multiple *in vitro* and *in vivo* studies which are explained by the contribution of each of the observed interfaces in complex formation and signaling.

DISCUSSION

Neuropilins were identified as receptors for class 3 semaphorins before plexins were found to be the signal transducing receptors for these as well as other classes of semaphorins⁸⁻¹¹. These initial and subsequent studies showed that the *Sema3s* interact directly with the *Nrps*, and that for *Sema3s* to trigger *PlxnA* signaling the plexin and *Nrp* must be associated as a holoreceptor. How does this holoreceptor complex differ from a direct semaphorin – plexin complex and in what way does *Nrp* mediate ligand – receptor signaling in this system? In combination our studies indicate that *Nrp* is needed to cement a weak, but canonical, interaction between *Sema3s* and *PlxnAs*. The generic architecture of the semaphorin-plexin interaction as established by studies on other family members^{6-7,15} is conserved. We and others have shown previously that semaphorin dimers are needed for signaling⁶⁻⁷ and the results presented here reveal that the core mechanism of semaphorin mediated plexin dimerization remains central to *Sema3* function.

Some twenty different semaphorins in higher vertebrates carry out a plethora of roles and the majority of these functions utilize one (or more) of the nine members of the plexin family of cell surface receptors for signal transduction. It is therefore perhaps unsurprising that a growing number of reports show diverse semaphorin ligands signal through the same plexin receptor to trigger very different cellular effects. The challenges posed for signal switching and fidelity are most apparent in the variety of biological functions mediated by *PlxnAs*. The *PlxnAs* bind multiple members of the class 3 and class 6 semaphorins. The *Sema3s* are secreted molecules and can modulate long-range effects on cellular processes by gradient formation (for example²⁶). Our results explain the central role of *Nrp*, and specifically the a1 domain, in *Sema3-PlxnA* signaling. We propose that the requirement for a1 as a cross-brace stabilizing the *Sema3-PlxnA* complex allows *Nrp* to gate signaling through the *PlxnA* receptors (Fig. 5), underpinning switches between *Sema3* and *Sema6* function such as recently reported for the osteoprotective activities of *Sema3A*³⁷. Similar to other semaphorin-plexin combinations, *Sema3* binding dimerizes and possibly clusters the plexin intracellular region leading to signaling. Whilst the role of *Nrp* as a co-receptor specifically stabilizing *Sema3-PlxnA* complexes is revealed here, the potential contribution of *Nrp* dimerization to clustering, and thus the properties of the signaling assembly, remains open.

Online Methods

Production of proteins

Mouse Sema3A_{S-P}, Sema3A_{S-P-I}, PlxnA2₁₋₄, Nrp1₁₋₄, Nrp1₁ and NRP1₂₋₄ (residues 21-568, 21-675, 35-703, 22-586, 22-144 and 143-586, respectively) were cloned into the pHLsec vector³⁹ with a C-terminal His-tag or a C-terminal biotin ligase (BirA) recognition sequence (for biotinylation⁴⁰ and subsequent SPR surface coupling). Sema3A is proteolytically processed at an internal furin site (F) (551RRTRR555)³⁰ in the PSI domain (P) and its C-terminal segment is removed during purification. The remaining N-terminal segment (residues 21-555) consists of the entire sema domain (S) and a large part of the PSI domain (P) and hence we denote this Sema3A version Sema3A_{S-F} (S-F for sema domain-furin site). To prevent Sema3A processing, and enable more controlled purification and sample homogeneity the furin site was mutated (R551A and R555A)^{30,41} in both the Sema3A_{S-P} and Sema3A_{S-P-I} constructs. For crystallization experiments proteins were expressed in HEK-293S cells⁴². For all other experiments proteins were expressed in HEK-293T cells with the exception of Nrp1₁ used as analyte in SPR experiments that was expressed in HEK-293S cells (Nrp1₁ does not contain N-linked glycosylation sites). Proteins were purified from buffer exchanged medium by immobilized metal-affinity and size-exclusion chromatography.

Crystallization and data collection

Nrp1₁₋₄ was concentrated to 5.9 mg/ml in 20 mM HEPES, pH 7.5, 150 mM NaCl and 2 mM CaCl₂. Prior to crystallization of the Sema3A_{S-F}-PlxnA2₁₋₄-Nrp1₁₋₄ complex individual components were mixed at a molar ratio of 1:1:1 and a final concentration of 6.9 mg/ml in 20 mM HEPES, pH 7.5, 150 mM NaCl and 2 mM CaCl₂ and subsequently deglycosylated with endoglycosidase F1⁴³. Sema3A_{S-P-I} (in which the furin site was mutated to R551A and R555A) was concentrated to 5.5 mg/ml in 20 mM HEPES, pH 7.5 and 150 mM NaCl. For crystallization of individual proteins Nrp1₁₋₄ and Sema3A_{S-P-I} were not deglycosylated. Sitting drop vapour diffusion crystallization trials were set up using a Cartesian Technologies pipetting robot and consisted of 100 nl (or for the complex 200 nl) protein solution and 100 nl reservoir solution⁴⁴. Crystallization plates were placed in a TAP Homebase storage vault maintained at 20.5 °C and imaged via a Veeco visualization system⁴⁵. Nrp1₁₋₄ was crystallized in 0.1 M HEPES, pH 7.5 and 1.5 M lithium sulphate, the Sema3A_{S-F}-PlxnA2₁₋₄-Nrp1₁₋₄ complex in 70 mM HEPES, pH 7.5, 1.4% w/v PEG400, 12% v/v glycerol, 1.4 M ammonium sulphate and either 1% v/v ethyl acetate, 8% v/v acetonitrile or nothing extra and Sema3A_{S-P-I} in 0.1 M sodium cacodylate, pH 5.5, 0.1 M calcium acetate and 12% w/v PEG8000. Before diffraction data collection crystals were soaked in mother liquor supplemented with 25% v/v ethylene glycol, 25% v/v glycerol or nothing extra for Nrp1₁₋₄, Sema3A_{S-P-I} and Sema3A_{S-F}-PlxnA2₁₋₄-Nrp1₁₋₄, respectively, and subsequently flash-cooled in liquid nitrogen. Data were collected at 100 K at Diamond beamlines I04-1 (Nrp1₁₋₄, Sema3A_{S-F}-PlxnA2₁₋₄-Nrp1₁₋₄ and Sema3A_{S-P-I}) and I02 and I03 (Sema3A_{S-F}-PlxnA2₁₋₄-Nrp1₁₋₄). Diffraction data (from one Nrp1₁₋₄ and Sema3A_{S-P-I} crystal each and three Sema3A_{S-F}-PlxnA2₁₋₄-Nrp1₁₋₄ crystals) were integrated, scaled and merged with MOSFLM⁴⁶ and AIMLESS in CCP4⁴⁷ (see Table 1).

Structure determination and refinement

We solved the structure of Nrp1₁₋₄ by molecular replacement in PHASER²⁸ using the structures of NRP1₂₋₄²³ (domains a2, b1 and b2) (PDB code 2QQM) and NRP2₁²³ (domain a1) (PDB code 2QQK) as a search models. This solution was completed by manual rebuilding in COOT⁴⁸ and refinement in REFMAC⁴⁹. The structure of the Sema3A_{S-F}-PlxnA2₁₋₄-Nrp1₁₋₄ complex was solved by molecular replacement in PHASER using the structures of PlxnA2₁₋₄⁶ (PDB code 3OKT), Sema3A_S¹³ (sema domain) (PDB code 1Q47)

and Nrp1₁ (domain a1) from the Nrp1₁₋₄ structure as search models. Nrp1 domains a2, b1 and b2 were omitted from the model due to disorder. The asymmetric unit contains six copies of PlxnA2₁₋₄ and one copy each of Sema3A_{S-F} and Nrp1₁₋₄ (see Supplementary Fig. 3). This solution was only subjected to rigid body refinement in PHENIX⁵⁰ with each domain as a rigid group (26 in total; four for each PlxnA2 molecule and one each for Sema3A and Nrp1) and a single B-factor per domain, thus preventing any overfitting. The structure of Sema3A_{S-P-I} was solved by molecular replacement in PHASER using the structure of Sema3A_S¹³ (PDB code 1Q47) as search model.

This solution was completed by manual rebuilding in COOT and refinement in REFMAC using local non-crystallography symmetry restraints throughout. The IG domain was only partially modelled and no residues have been assigned to this domain due to disorder. Refinement statistics are given in Table 1. Ramachandran statistics are as follows (favored/disallowed (%)): Nrp1₁₋₄ 95.5/0.9, Sema3A_{S-F}-PlxnA2₁₋₄-Nrp1₁₋₄ 96.4/0.7 and Sema3A_{S-P-I} 91.7/0.37. Overall MOLPROBITY⁵¹ scores are as follows (percentile, with 100th percentile the best among structures of comparable resolution): Nrp1₁₋₄ 98th, Sema3A_{S-F}-PlxnA2₁₋₄-Nrp1₁₋₄ 99th and Sema3A_{1-4 S-P-I} 99th. Electrostatics potentials were generated using PDB2PQR⁵² and APBS⁵³, alignments were calculated using ClustalW⁵⁴, residue conservedness was calculated with ConSurf⁵⁵ and buried surface areas of protein-protein interactions were calculated using PISA⁵⁶. Figures were produced using PyMOL (<http://www.pymol.org>).

Site-directed mutagenesis

In addition to the Sema3A furin site mutations (R551A and R555A) in the Sema3A_{S-P} and Sema3A_{S-P-I} constructs several protein-protein interface mutants were generated that introduce a glycosylation site; Sema3A_{S-P} L353N P355S in the Nrp1 binding site, PlxnA2₁₋₄F275N in the Nrp1 binding site and Nrp1₁₋₄ P73A H74S in the Sema3A binding site (see Fig. 2c). These were cloned into the pHLsec mammalian expression vector, resulting in protein constructs with a C-terminal hexahistidine tag³⁹ or a C-terminal BirA recognition sequence for biotinylation⁴⁰. All mutant proteins were expressed in HEK-293T cells to ensure full glycosylation.

Multiangle light scattering

A MALS experiment with Nrp1₁₋₄ was performed during size exclusion chromatography on an analytical Superdex S200 10:30 column (GE Healthcare) with online static light-scattering (DAWN HELEOS II, Wyatt Technology), differential refractive index (Optilab rEX, Wyatt Technology) and Agilent 1200 UV (Agilent Technologies) detectors. Data were analyzed using the ASTRA software package (Wyatt Technology).

Surface plasmon resonance equilibrium binding studies

SPR-based protein-protein interaction studies were performed using a Biacore T100 instrument (GE Healthcare) in 150 mM NaCl, 10 mM HEPES pH 7.5, 0.005 % (v/v) Tween 20 running buffer at 25 °C. The Biacore T100 analyte compartment was kept at 20 °C (except for the experiment with EDTA in Fig. 4a and Supplementary Fig. 6d where the compartment temperature was kept at 10 °C). Biotinylated ligands were immobilized on a CM5 Biacore sensor chip surface (~1000-5000 RU of streptavidin; Thermo Fisher Scientific Inc.). Sema3A_{S-P} or mutants thereof (thus including the furin site mutations, R551A and R555A) were used in the SPR experiments except for the experiment shown in Fig. 4a right bottom panel and Supplementary Fig. 6d (with EDTA) in which the processed form (Sema3A_{S-F}) was used. In all experiments analytes in SPR running buffer were supplemented with CaCl₂, pH ~7.5 (final concentration 2 mM) or EDTA, pH 7.5 (Fig. 4a right bottom panel and Supplementary Fig. 6d, final concentration 2 mM) immediately

before use. Analyte concentrations were determined from the absorbance at 280 nm using molar extinction coefficients calculated with ProtParam⁵⁷. For measurements of analyte binding to immobilized ligands, samples were injected at 5 $\mu\text{l min}^{-1}$. The signal from experimental flow cells was corrected by subtraction of a buffer and reference signal from a control flow cell coated with streptavidin only. After each injection, the sensor surface was regenerated using 2 M MgCl_2 (100 $\mu\text{l min}^{-1}$, 1 min). Apparent dissociation constants (K_d) and maximum analyte binding (B_{max}) values were calculated using Scrubber2 (BioLogic Software) by nonlinear curve fitting of a 1:1 Langmuir binding isotherm model ($\text{bound} = C * B_{\text{max}} / (K_d + C)$, where C is the analyte concentration). In experiments with Sema3A or a Sema3A-Nrp1 combination as analyte, binding may not fit well to a 1:1 model due to mixed bivalent and monovalent or more complex interactions. Apparent K_d values calculated in these experiments are therefore approximations. Nevertheless, apparent affinities of wild-type and mutant proteins can be compared relative to each other.

Growth cone collapse assays

All animal studies were performed according to the United Kingdom Home Office Animals Act (1986). Dissociated dorsal root ganglion cultures were generated from 4-8 week old CD1 mice as previously described⁵⁸. Cells were maintained overnight in DMEM F-12 supplemented with 10% FCS, penicillin-streptomycin mix and 0.1 ng/ml NGF. Sema3A_{S-P}, Sema3A_{S-pL353N P355S}, or vehicle was applied to the cell medium at a concentration of 10 nM or 100 nM for 30 minutes at 37 °C. Cells were then fixed in 4% paraformaldehyde containing 10% sucrose. The actin cytoskeleton was visualised with rhodamine phalloidin and growth cone collapse was assessed as described⁵⁹. In brief, experiments were scored for the number of intact and collapsed growth cones with an intact cone defined as a neurite, ending in a flattened lamellipodia and/or two or more filopodia. Collapsed cones have a bullet-shaped tip and no more than one filopodia.

Supplementary Material

Refer to Web version on PubMed Central for supplementary material.

Acknowledgments

We thank the staff of Diamond beamlines I02, I03 and I04-1 for assistance with diffraction data collection, Y. Zhao and W. Lu for help with protein expression, T.S. Walter for help with crystallization, G. Sutton for help with MALS experiments A.R. Aricescu and D.I. Stuart for critical reading of the manuscript. This work was funded by Cancer Research UK (A10976) and the Medical Research Council (G9900061) to E.Y.J.. B.J.C.J. is funded by the Human Frontier Science Program, G.A.W. and M.Z.C. are funded by the Medical Research Council and the John Fell Fund, C.S. is funded by the Wellcome Trust and E.Y.J. by Cancer Research UK (A5261).

References

1. Kolodkin AL, Tessier-Lavigne M. Mechanisms and molecules of neuronal wiring: a primer. *Cold Spring Harb Perspect Biol.* 2011; 3
2. Tran TS, Kolodkin AL, Bharadwaj R. Semaphorin regulation of cellular morphology. *Annu Rev Cell Dev Biol.* 2007; 23:263–292. [PubMed: 17539753]
3. Zhou Y, Gunput RA, Pasterkamp RJ. Semaphorin signaling: progress made and promises ahead. *Trends Biochem Sci.* 2008; 33:161–170. [PubMed: 18374575]
4. Takamatsu H, Kumanogoh A. Diverse roles for semaphorin-plexin signaling in the immune system. *Trends Immunol.* 2012; 33:127–135. [PubMed: 22325954]
5. Muratori C, Tamagnone L. Semaphorin signals tweaking the tumor microenvironment. *Adv Cancer Res.* 2012; 114:59–85. [PubMed: 22588056]
6. Janssen BJ, et al. Structural basis of semaphorin-plexin signalling. *Nature.* 2010; 467:1118–1122. [PubMed: 20877282]

7. Nogi T, et al. Structural basis for semaphorin signalling through the plexin receptor. *Nature*. 2010; 467:1123–1127. [PubMed: 20881961]
8. He Z, Tessier-Lavigne M. Neuropilin is a receptor for the axonal chemorepellent Semaphorin III. *Cell*. 1997; 90:739–751. [PubMed: 9288753]
9. Kolodkin AL, et al. Neuropilin is a semaphorin III receptor. *Cell*. 1997; 90:753–762. [PubMed: 9288754]
10. Tamagnone L, et al. Plexins are a large family of receptors for transmembrane, secreted, and GPI-anchored semaphorins in vertebrates. *Cell*. 1999; 99:71–80. [PubMed: 10520995]
11. Takahashi T, et al. Plexin-neuropilin-1 complexes form functional semaphorin-3A receptors. *Cell*. 1999; 99:59–69. [PubMed: 10520994]
12. Soker S, Takashima S, Miao HQ, Neufeld G, Klagsbrun M. Neuropilin-1 is expressed by endothelial and tumor cells as an isoform-specific receptor for vascular endothelial growth factor. *Cell*. 1998; 92:735–745. [PubMed: 9529250]
13. Antipenko A, et al. Structure of the semaphorin-3A receptor binding module. *Neuron*. 2003; 39:589–598. [PubMed: 12925274]
14. Love CA, et al. The ligand-binding face of the semaphorins revealed by the high-resolution crystal structure of SEMA4D. *Nat Struct Biol*. 2003; 10:843–848. [PubMed: 12958590]
15. Liu H, et al. Structural basis of semaphorin-plexin recognition and viral mimicry from Sema7A and A39R complexes with PlexinC1. *Cell*. 2010; 142:749–761. [PubMed: 20727575]
16. Tong Y, et al. Structure and function of the intracellular region of the plexin-b1 transmembrane receptor. *J Biol Chem*. 2009; 284:35962–35972. [PubMed: 19843518]
17. He H, Yang T, Terman JR, Zhang X. Crystal structure of the plexin A3 intracellular region reveals an autoinhibited conformation through active site sequestration. *Proc Natl Acad Sci U S A*. 2009; 106:15610–15615. [PubMed: 19717441]
18. Bell CH, Aricescu AR, Jones EY, Siebold C. A dual binding mode for RhoGTPases in plexin signalling. *PLoS Biol*. 2011; 9:e1001134. [PubMed: 21912513]
19. Wang Y, et al. Plexins are GTPase-activating proteins for Rap and are activated by induced dimerization. *Sci Signal*. 2012; 5:ra6. [PubMed: 22253263]
20. Chen H, He Z, Bagri A, Tessier-Lavigne M. Semaphorin-neuropilin interactions underlying sympathetic axon responses to class III semaphorins. *Neuron*. 1998; 21:1283–1290. [PubMed: 9883722]
21. Giger RJ, et al. Neuropilin-2 is a receptor for semaphorin IV: insight into the structural basis of receptor function and specificity. *Neuron*. 1998; 21:1079–1092. [PubMed: 9856463]
22. Nakamura F, Tanaka M, Takahashi T, Kalb RG, Strittmatter SM. Neuropilin-1 extracellular domains mediate semaphorin D/III-induced growth cone collapse. *Neuron*. 1998; 21:1093–1100. [PubMed: 9856464]
23. Appleton BA, et al. Structural studies of neuropilin/antibody complexes provide insights into semaphorin and VEGF binding. *Embo J*. 2007; 26:4902–4912. [PubMed: 17989695]
24. Gaur P, et al. Role of class 3 semaphorins and their receptors in tumor growth and angiogenesis. *Clin Cancer Res*. 2009; 15:6763–6770. [PubMed: 19887479]
25. Rohm B, Ottemeyer A, Lohrum M, Puschel AW. Plexin/neuropilin complexes mediate repulsion by the axonal guidance signal semaphorin 3A. *Mech Dev*. 2000; 93:95–104. [PubMed: 10781943]
26. Chen G, et al. Semaphorin-3A guides radial migration of cortical neurons during development. *Nat Neurosci*. 2008; 11:36–44. [PubMed: 18059265]
27. Takahashi T, Strittmatter SM. PlexinA1 autoinhibition by the plexin sema domain. *Neuron*. 2001; 29:429–439. [PubMed: 11239433]
28. McCoy AJ, et al. Phaser crystallographic software. *J Appl Crystallogr*. 2007; 40:658–674. [PubMed: 19461840]
29. Toyofuku T, et al. Repulsive and attractive semaphorins cooperate to direct the navigation of cardiac neural crest cells. *Dev Biol*. 2008; 321:251–262. [PubMed: 18625214]
30. Adams RH, Lohrum M, Klostermann A, Betz H, Puschel AW. The chemorepulsive activity of secreted semaphorins is regulated by furin-dependent proteolytic processing. *Embo J*. 1997; 16:6077–6086. [PubMed: 9321387]

31. Parker MW, Hellman LM, Xu P, Fried MG, Vander Kooi CW. Furin processing of semaphorin 3F determines its anti-angiogenic activity by regulating direct binding and competition for neuropilin. *Biochemistry*. 2010; 49:4068–4075. [PubMed: 20387901]
32. Merte J, et al. A forward genetic screen in mice identifies Sema3A(K108N), which binds to neuropilin-1 but cannot signal. *J Neurosci*. 2010; 30:5767–5775. [PubMed: 20410128]
33. Ueyama H, et al. Semaphorin 3A lytic hybrid peptide binding to neuropilin-1 as a novel anti-cancer agent in pancreatic cancer. *Biochem Biophys Res Commun*. 2011; 414:60–66. [PubMed: 21945444]
34. Shirvan A, et al. Semaphorins as mediators of neuronal apoptosis. *J Neurochem*. 1999; 73:961–971. [PubMed: 10461885]
35. Shirvan A, et al. Anti-semaphorin 3A antibodies rescue retinal ganglion cells from cell death following optic nerve axotomy. *J Biol Chem*. 2002; 277:49799–49807. [PubMed: 12376549]
36. Gu C, et al. Characterization of neuropilin-1 structural features that confer binding to semaphorin 3A and vascular endothelial growth factor 165. *J Biol Chem*. 2002; 277:18069–18076. [PubMed: 11886873]
37. Hayashi M, et al. Osteoprotection by semaphorin 3A. *Nature*. 2012; 485:69–74. [PubMed: 22522930]
38. Roth L, et al. Transmembrane domain interactions control biological functions of neuropilin-1. *Mol Biol Cell*. 2008; 19:646–654. [PubMed: 18045991]
39. Aricescu AR, Lu W, Jones EY. A time- and cost-efficient system for high-level protein production in mammalian cells. *Acta Crystallogr D Biol Crystallogr*. 2006; 62:1243–1250. [PubMed: 17001101]
40. O’Callaghan CA, et al. BirA enzyme: production and application in the study of membrane receptor-ligand interactions by site-specific biotinylation. *Anal Biochem*. 1999; 266:9–15. [PubMed: 9887208]
41. Koppel AM, Feiner L, Kobayashi H, Raper JA. A 70 amino acid region within the semaphorin domain activates specific cellular response of semaphorin family members. *Neuron*. 1997; 19:531–537. [PubMed: 9331346]
42. Reeves PJ, Callewaert N, Contreras R, Khorana HG. Structure and function in rhodopsin: high-level expression of rhodopsin with restricted and homogeneous N-glycosylation by a tetracycline-inducible N-acetylglucosaminyltransferase I-negative HEK293S stable mammalian cell line. *Proc Natl Acad Sci U S A*. 2002; 99:13419–13424. [PubMed: 12370423]
43. Chang VT, et al. Glycoprotein structural genomics: solving the glycosylation problem. *Structure*. 2007; 15:267–273. [PubMed: 17355862]
44. Walter TS, et al. A procedure for setting up high-throughput nanolitre crystallization experiments. Crystallization workflow for initial screening, automated storage, imaging and optimization. *Acta Crystallogr D Biol Crystallogr*. 2005; 61:651–657. [PubMed: 15930615]
45. Mayo CJ, et al. Benefits of automated crystallization plate tracking, imaging, and analysis. *Structure*. 2005; 13:175–182. [PubMed: 15698562]
46. Leslie AG. Recent changes to the MOSFLM package for processing film and image plate data. *Joint CCP4⁺ ESF-EAMCB Newsletter on Protein Crystallography*. 1992:26.
47. CCP4. The CCP4 suite: programs for protein crystallography. *Acta Crystallogr D Biol Crystallogr*. 1994; 50:760–763. [PubMed: 15299374]
48. Emsley P, Cowtan K. Coot: model-building tools for molecular graphics. *Acta Crystallogr D Biol Crystallogr*. 2004; 60:2126–2132. [PubMed: 15572765]
49. Murshudov GN, Vagin AA, Dodson EJ. Refinement of macromolecular structures by the maximum-likelihood method. *Acta Crystallogr D Biol Crystallogr*. 1997; 53:240–255. [PubMed: 15299926]
50. Adams PD, et al. PHENIX: building new software for automated crystallographic structure determination. *Acta Crystallogr D Biol Crystallogr*. 2002; 58:1948–1954. [PubMed: 12393927]
51. Davis IW, et al. MolProbity: all-atom contacts and structure validation for proteins and nucleic acids. *Nucleic Acids Res*. 2007; 35:W375–383. [PubMed: 17452350]

52. Dolinsky TJ, Nielsen JE, McCammon JA, Baker NA. PDB2PQR: an automated pipeline for the setup of Poisson-Boltzmann electrostatics calculations. *Nucleic Acids Res.* 2004; 32:W665–667. [PubMed: 15215472]
53. Baker NA, Sept D, Joseph S, Holst MJ, McCammon JA. Electrostatics of nanosystems: application to microtubules and the ribosome. *Proc Natl Acad Sci U S A.* 2001; 98:10037–10041. [PubMed: 11517324]
54. Larkin MA, et al. Clustal W and Clustal X version 2.0. *Bioinformatics.* 2007; 23:2947–2948. [PubMed: 17846036]
55. Landau M, et al. ConSurf 2005: the projection of evolutionary conservation scores of residues on protein structures. *Nucleic Acids Res.* 2005; 33:W299–302. [PubMed: 15980475]
56. Krissinel E, Henrick K. Inference of macromolecular assemblies from crystalline state. *J Mol Biol.* 2007; 372:774–797. [PubMed: 17681537]
57. Gasteiger E, et al. ExPASy: The proteomics server for in-depth protein knowledge and analysis. *Nucleic Acids Res.* 2003; 31:3784–3788. [PubMed: 12824418]
58. Malin SA, Davis BM, Molliver DC. Production of dissociated sensory neuron cultures and considerations for their use in studying neuronal function and plasticity. *Nat Protoc.* 2007; 2:152–160. [PubMed: 17401349]
59. Kapfhammer JP, Xu H, Raper JA. The detection and quantification of growth cone collapsing activities. *Nat Protoc.* 2007; 2:2005–2011. [PubMed: 17703212]

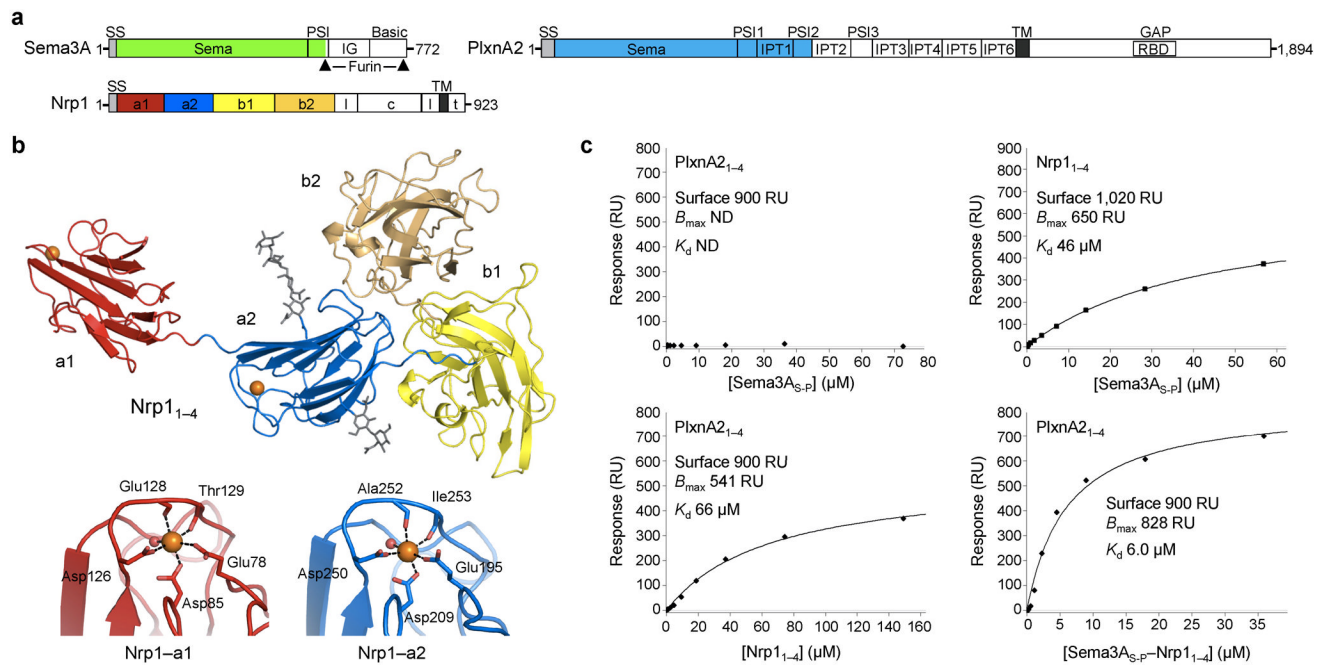


Figure 1. Nrp1 locks Sema3A and PlxnA2 together

a, Schematic domain organisation of mouse Sema3A, PlxnA2 and Nrp1. SS: signal sequence, TM: transmembrane region, I: linker, t: tail, GAP: GTPase activating protein, RBD: Rho GTPase-binding domain. Arrows indicate furin processing sites in Sema3A. The domains included in the crystallization constructs are colored. **b**, Ribbon representation of Nrp1₁₋₄, Ca²⁺ ions shown as orange spheres and N-linked glycans shown in grey stick representation (top panel). Detailed view of the two Ca²⁺ binding sites in Nrp1 with coordinating residues in stick representation and waters as small red spheres (bottom panels). **c**, SPR equilibrium experiments indicate no or very little interaction between Sema3A_{S-P}-PlxnA2₁₋₄, direct interaction between Sema3A_{S-P}-Nrp1₁₋₄ and PlxnA2₁₋₄-Nrp1₁₋₄ and an added effect upon interaction of all three (Sema3A_{S-P}-PlxnA2₁₋₄-Nrp1₁₋₄) components.

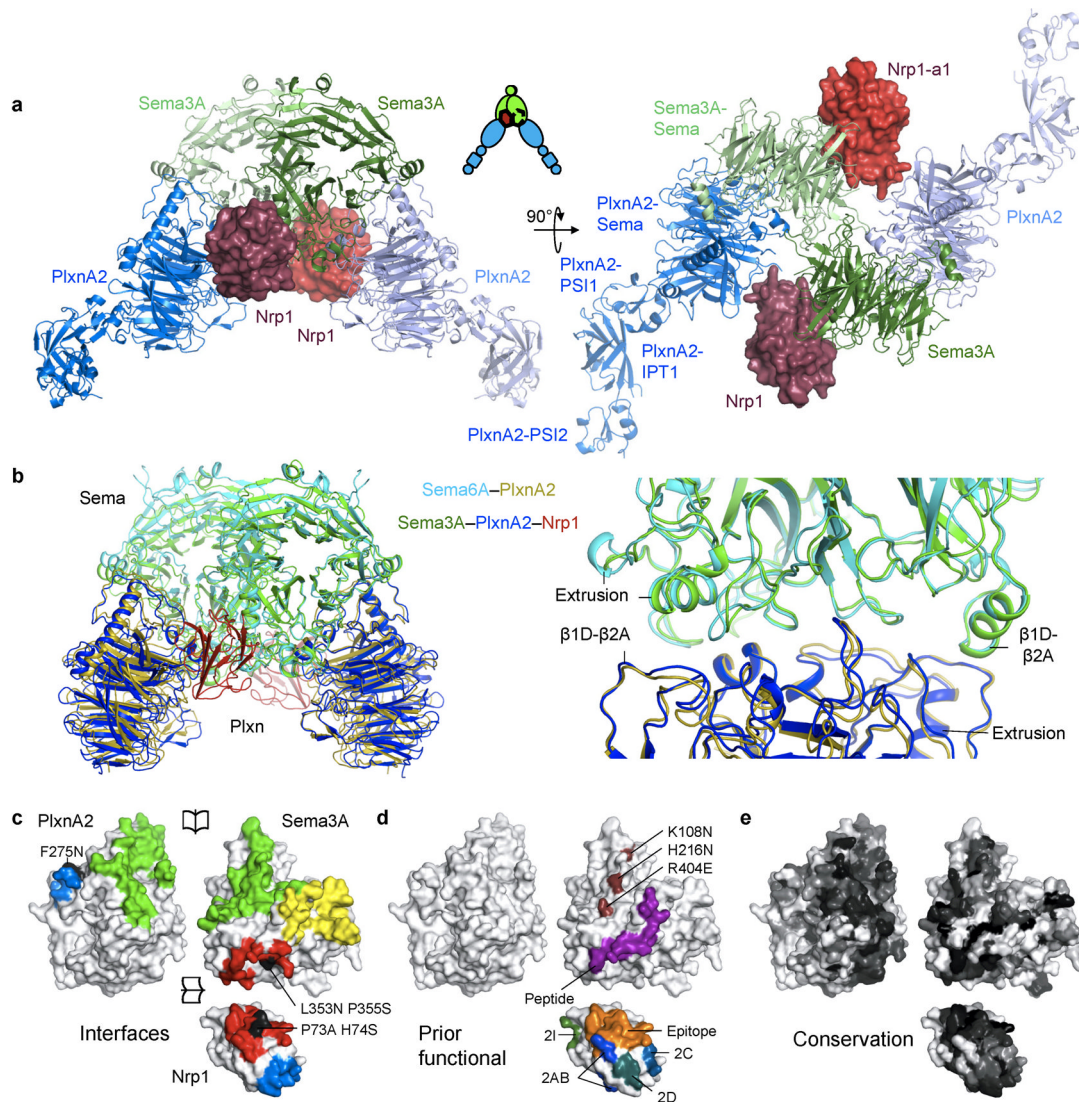


Figure 2. Complex architecture and interfaces are conserved and validated

a, The Sema3A_{S-F}-PlxnA2₁₋₄-Nrp1₁₋₄ complex with Sema3A and PlxnA2 in ribbon representation, Nrp1 in surface representation and a schematic drawing (middle panel). **b**, Ribbon representation of Sema3A-PlxnA2-Nrp1 superposed onto Sema6A-PlxnA2⁶ (Protein Data Bank (PDB) code 3OKY) based on the sema domains of a Sema3A and Sema6A molecule (left) and enlargement (right). **c-e**, Opened view. **c**, Interfaces of Sema3A-PlxnA2 (green), Sema3A-Nrp1 (red), Nrp1-PlxnA2 (blue) and Sema3A-Sema3A (yellow) and interface mutants used in biophysical and cellular assays (black). **d**, Mapping of previous interaction data: Sema3A mutations K108N³², H216N and R404E⁷ (ruby), Sema3A derived peptide 363-380 (ref. 33) (purple), Nrp1 mutations (2AB, 2C, 3D, 2I)³⁶ color-coded from most disrupting Sema3A binding (blue) to no effect (green) and a Nrp1 epitope²³ (orange). **e**, Sema3A, PlxnA2 and Nrp1 color-coded according to residue conservation (from non-conserved, white, to conserved, black) based on alignments containing sequences from all vertebrate Sema3 and PlxnA class members and all Nrps. In **b-e** only the sema domains and Nrp1 domain a1 are shown.

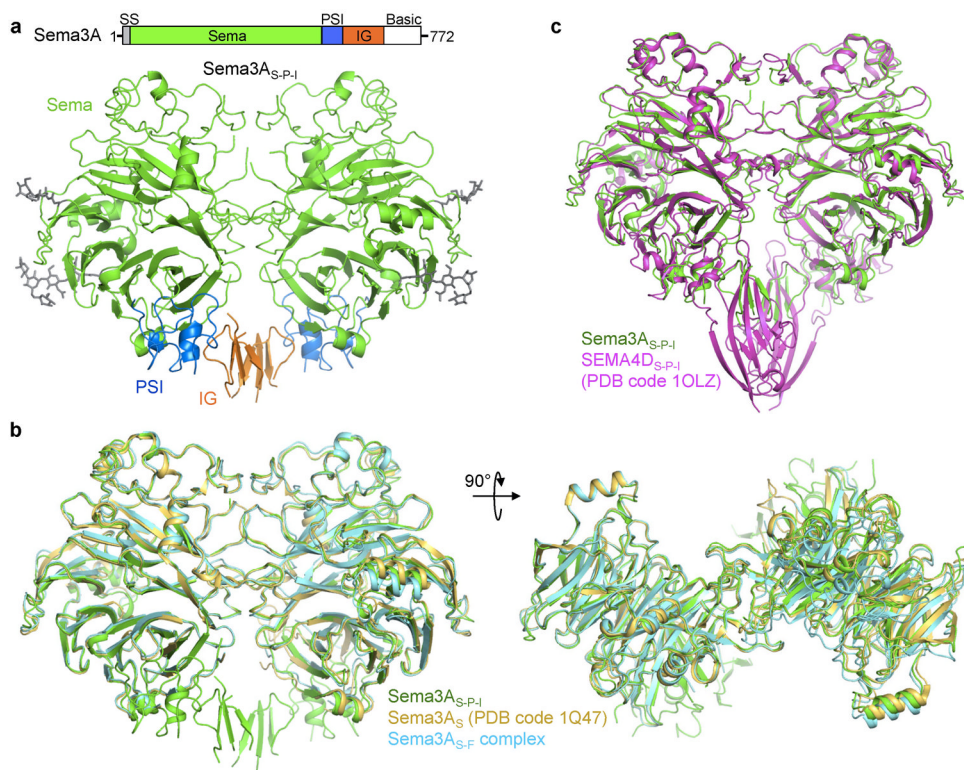


Figure 3. The structure of Sema3A_{S-P-I} is very similar to that of Sema4D_{S-P-I}
a, Crystal structure of Sema3A_{S-P-I} in which the furin site (551RRTRR555) was mutated to R551A and R555A. The IG domain is only partially modelled. N-linked glycans are shown in grey stick representation. **b**, Superpositions of Sema3A_{S-P-I} with unliganded Sema3A_S (PDB code 1Q47)¹³ and Sema3A_{S-F} from the Sema3A-PlxnA2-Nrp1 complex described here. **c**, Superposition of Sema3A_{S-P-I} and SEMA4D_{S-P-I} (PDB code 1OLZ)¹⁴.

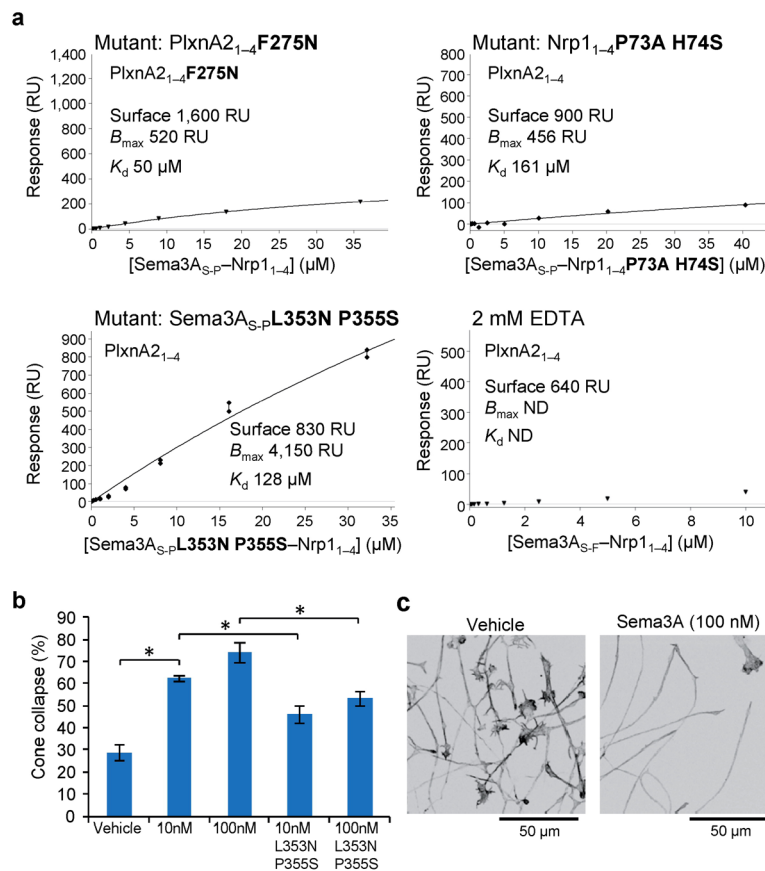


Figure 4. Interface mutants have reduced interaction and activity

a, Interface mutations (see also Fig. 2c and Supplementary Fig. 6) or sequestering of Ca²⁺ (by EDTA) reduce interactions between proteins. **b**, Mutant Sema3A has reduced collapse-inducing activity. Adult mouse DRG were incubated with Sema3A_{S-P}, Sema3A_{S-P}L353N P355S (both at 10 and 100 nM) or vehicle and scored for numbers of intact and collapsed growth cones. For each experimental condition at least 200 growth cones were used. Each data point is the mean ± s.e.m. of several independent experiments (6 for vehicle, 4 for 10 nM wt Sema3A, 3 for 100 nM wt Sema3A, 5 for 10 nM mutant Sema3A and 5 for 100 nM mutant Sema3A). (*p<0.05 by unpaired *t*-test). **c**, Representative images of non-collapsed (left panel) and Sema3A_{S-P} collapsed (right panel) DRG growth cones. Scale bar, 50 μm.

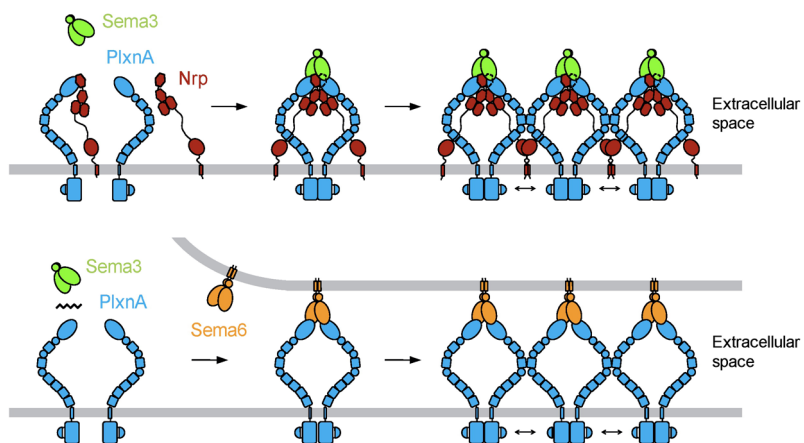


Figure 5. Model for secreted Sema3-PlxnA-Nrp and cell-surface bound Sema6-PlxnA signaling Nrp and PlxnA can form *cis* complexes independent of Sema3 binding. Binding of Sema3 further stabilizes Nrp-PlxnA interaction and induces PlxnA2 dimerization. Nrp-Nrp interaction via the MAM domain²⁰⁻²², transmembrane helix³⁸ or PlxnA-PlxnA interaction⁶ may seed further oligomerization (top panel). In absence of Nrp, PlxnA cannot signal via Sema3 but retains the ability to signal via membrane bound Sema6 (bottom panel).

Table 1

Data collection and refinement statistics

	Nrp1 ₁₋₄	Sema3A _S - F-PlxnA2 ₁₋₄ -Nrp1 ₁₋₄ [#]	Sema3A _{S,P.1}
Data collection			
Space group	<i>P</i> 321	<i>C</i> 2	<i>P</i> 2 ₁ 2 ₁ 2 ₁
Cell dimensions			
<i>a</i> , <i>b</i> , <i>c</i> (Å)	245.4, 245.4, 47.9	191.6, 293.6, 252.2	97.6, 126.2, 161.5
<i>α</i> , <i>β</i> , <i>γ</i> (°)	90, 90, 120	90, 106.4, 90	90, 90, 90
Resolution (Å)	81–2.7 (2.79–2.70) [*]	126–7.0 (7.67–7.00) [*]	77–3.3 (3.48–3.30) [*]
<i>R</i> _{merge} (%)	10.8 (66.0)	16.1 (52.9)	20.2 (59.4)
<i>I</i> / <i>σI</i>	8.4 (1.6)	7.3 (2.5)	5.2 (2.0)
Completeness (%)	99.4 (99.6)	95.6 (97.1)	97.7 (99.0)
Redundancy	5.0 (4.5)	5.1 (5.1)	3.5 (3.6)
Refinement			
Resolution (Å)	81–2.7	126–7.0	77–3.3
No. reflections	45078	20176	29876
<i>R</i> _{work} / <i>R</i> _{free} (%)	19.9/22.3	28.5/28.5	21.3/26.5
No. atoms			
Protein	4549	35655	8903
Ligand/ion	24	1	8
Water	29	0	0
B-factors (Å ²)			
Protein	68.2	323.2	55.9
Ligand/ion	83.9	369.5	58.5
Water	51.1	–	–
R.m.s deviations			
Bond lengths (Å)	0.009	0.014	0.011
Bond angles (°)	1.58	1.2	1.56

*R*_{free} is based on 5% of the total reflections.

^{*} Highest resolution shell is shown in parenthesis.

[#] Diffraction data from three crystals were used.